SUPPORTING INFORMATION

Exploring the Balance between Spin Frustration and Single-Ion Effects in Triangular Dy_3 Complexes.

Chieh-Wei Chang,[a] Jérôme Rouquette, [b] Po-Heng Lin*[a] and Jérôme Long*[b, c]

a. Department of Chemistry, National Chung Hsing University, Taichung 402, Taiwan. E-mail: poheng@dragon.nchu.edu.tw

b. ICGM, Univ. Montpellier, CNRS, ENSCM, Montpellier, France. E-mail: jerome.long@umontpellier.fr

c. Institut Universitaire de France (IUF), 1 rue Descartes, 75231 Paris Cedex 05, France.

TABLE OF CONTENTS

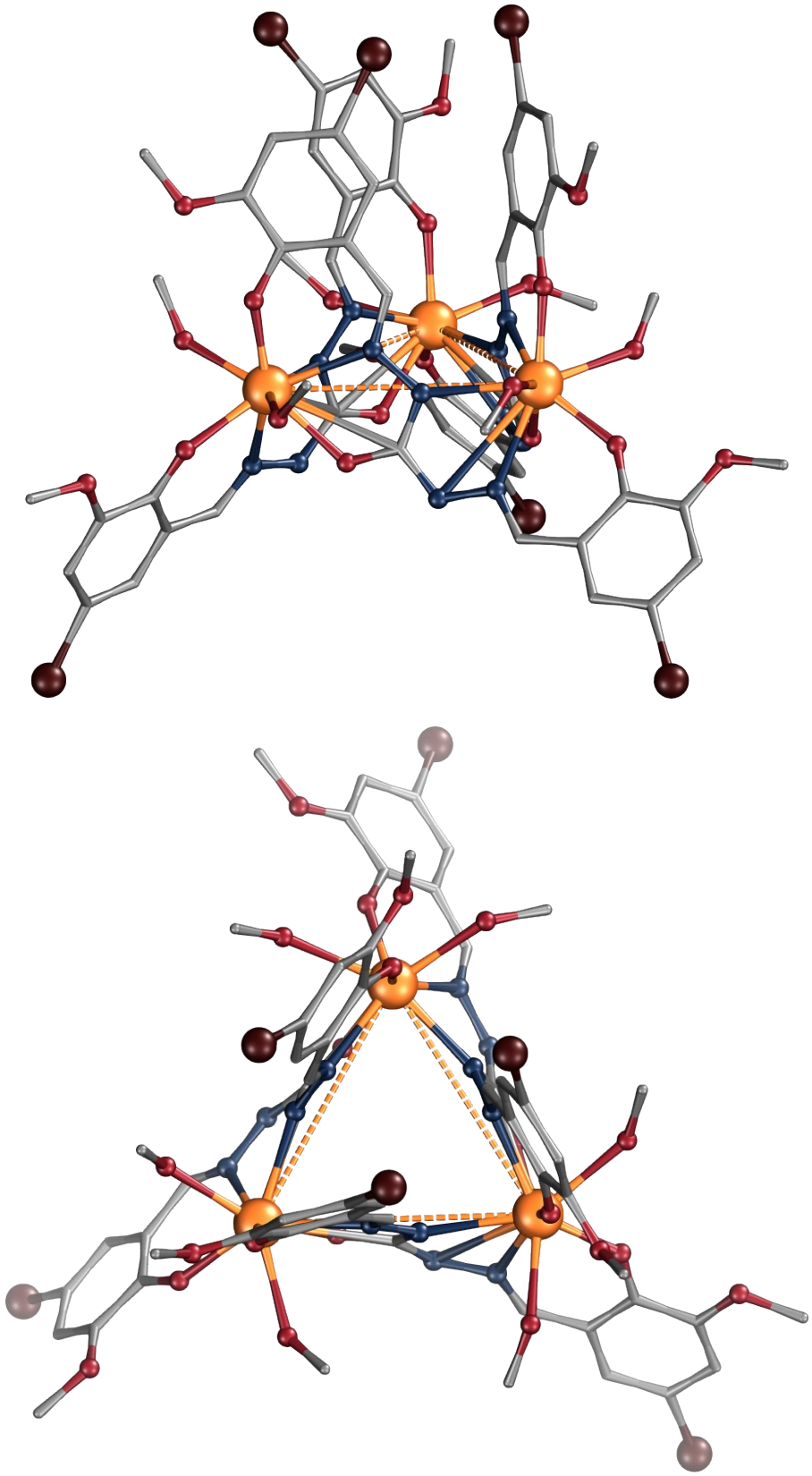

Figure S1: a) Molecular structures of **2**. Colour code: orange, Dy; red, O; blue, N; grey, C.;dark red, Br. Hydrogen atoms have been omitted for clarity. View from the top of the Dy_3 triangle arrangement.

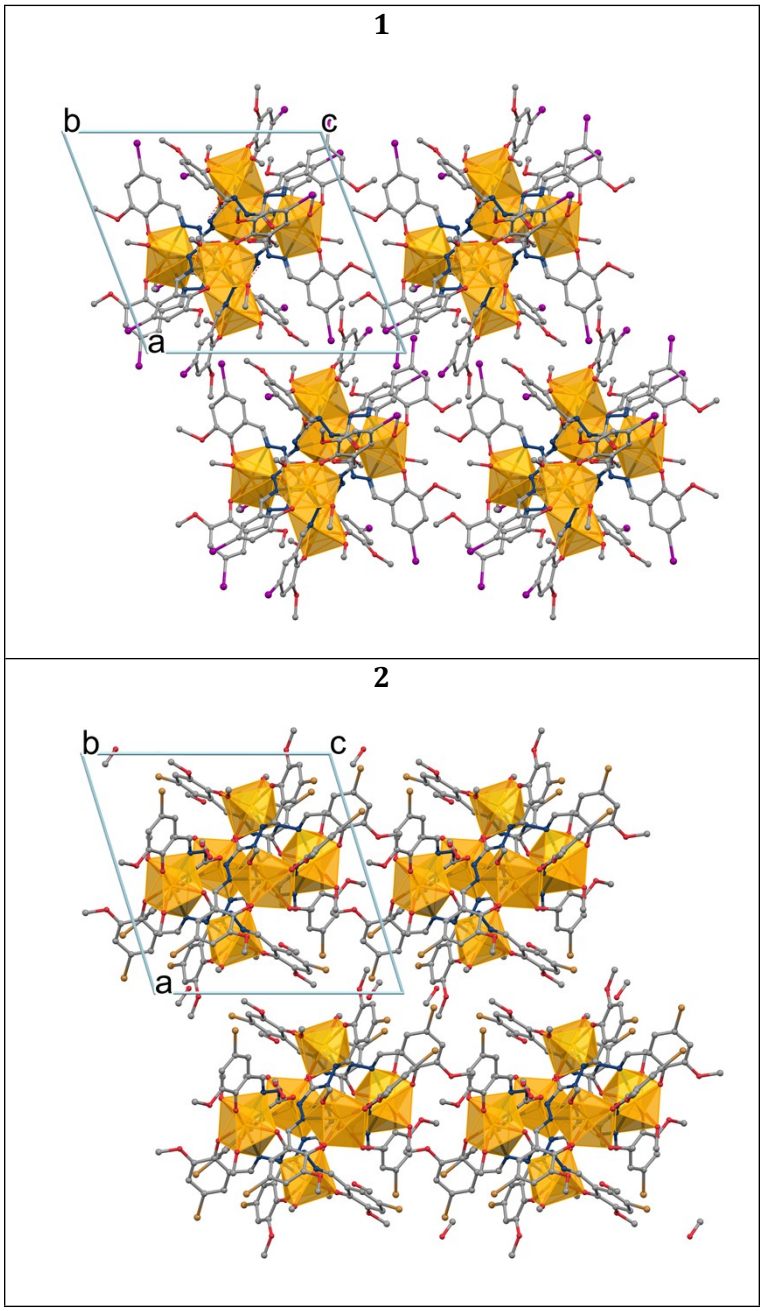

Figure S2: Views of the packing arrangements for complexes **1** and **2** along the *b* crystallographic axis. The hydrogen atoms have been omitted for clarity.

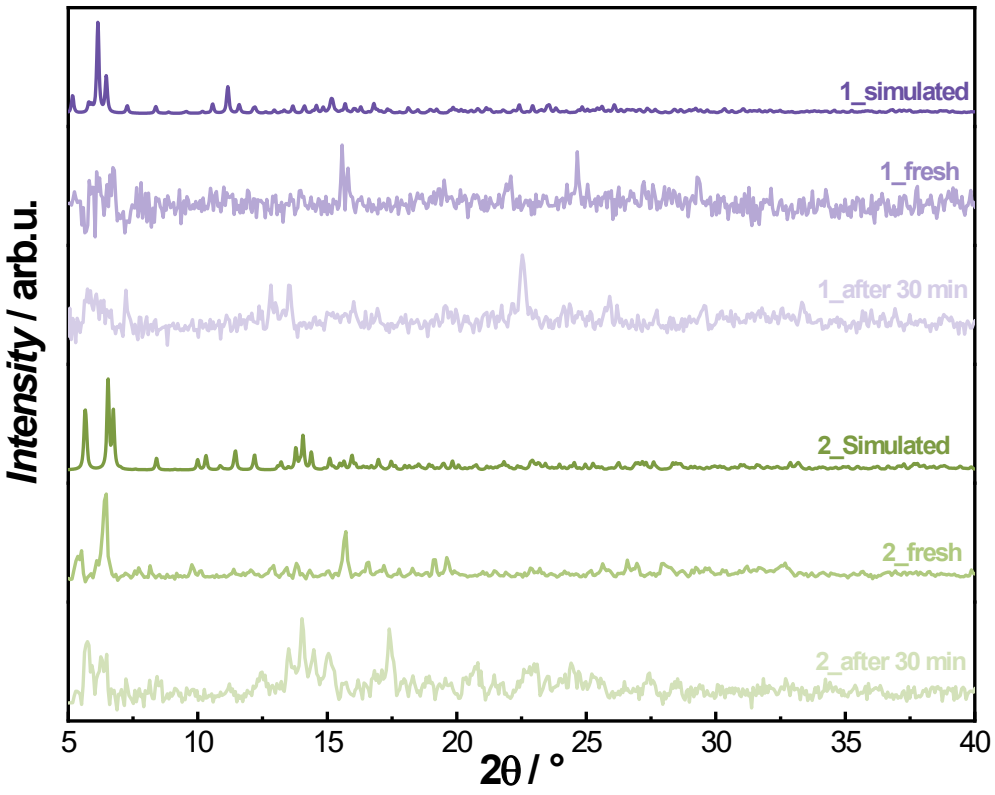

Figure S3: PXRD patterns for **1** and **2**.

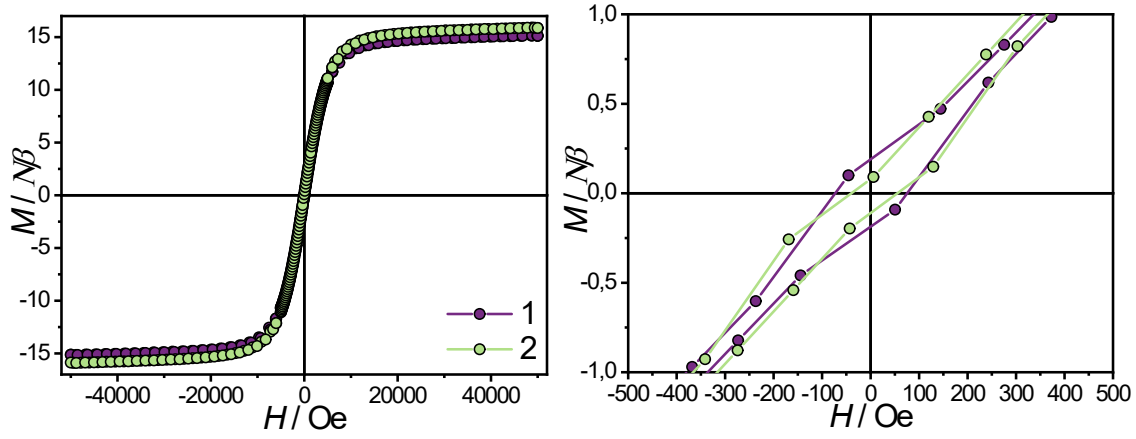

Figure S4: Hysteresis loops measured at 1.8 K using a magnetic field sweep rate of 25 Oe/s (-5000 to 5000 range).

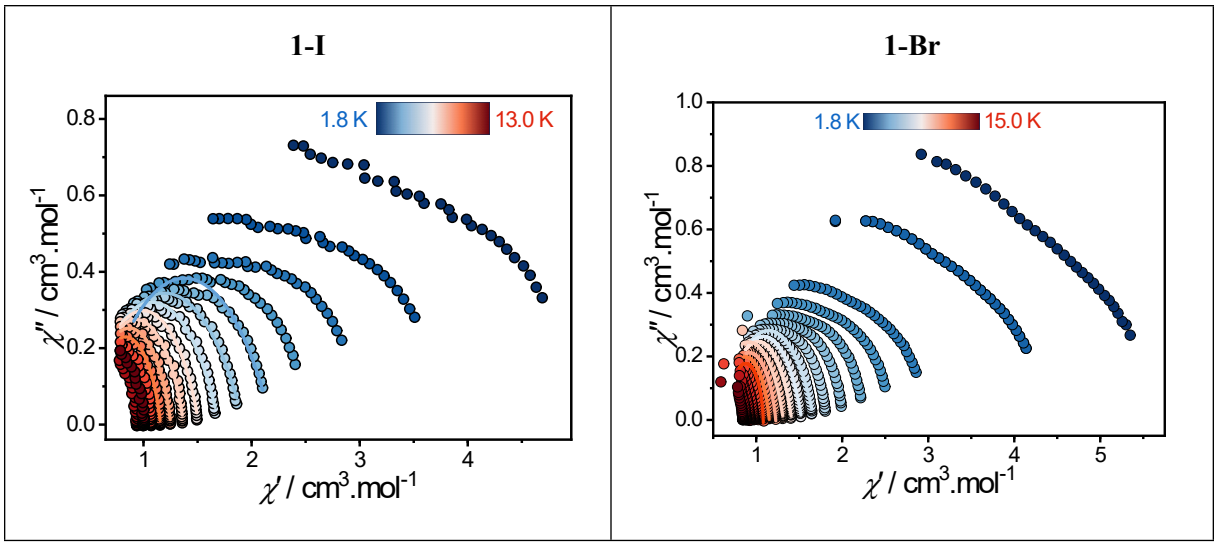

Figure S5: Cole-Cole (Argand) plots obtained using the ac susceptibility data for 1-I and 2-Br under a 0 Oe dc field. The solid lines correspond to the fit obtained with a generalized Debye model.

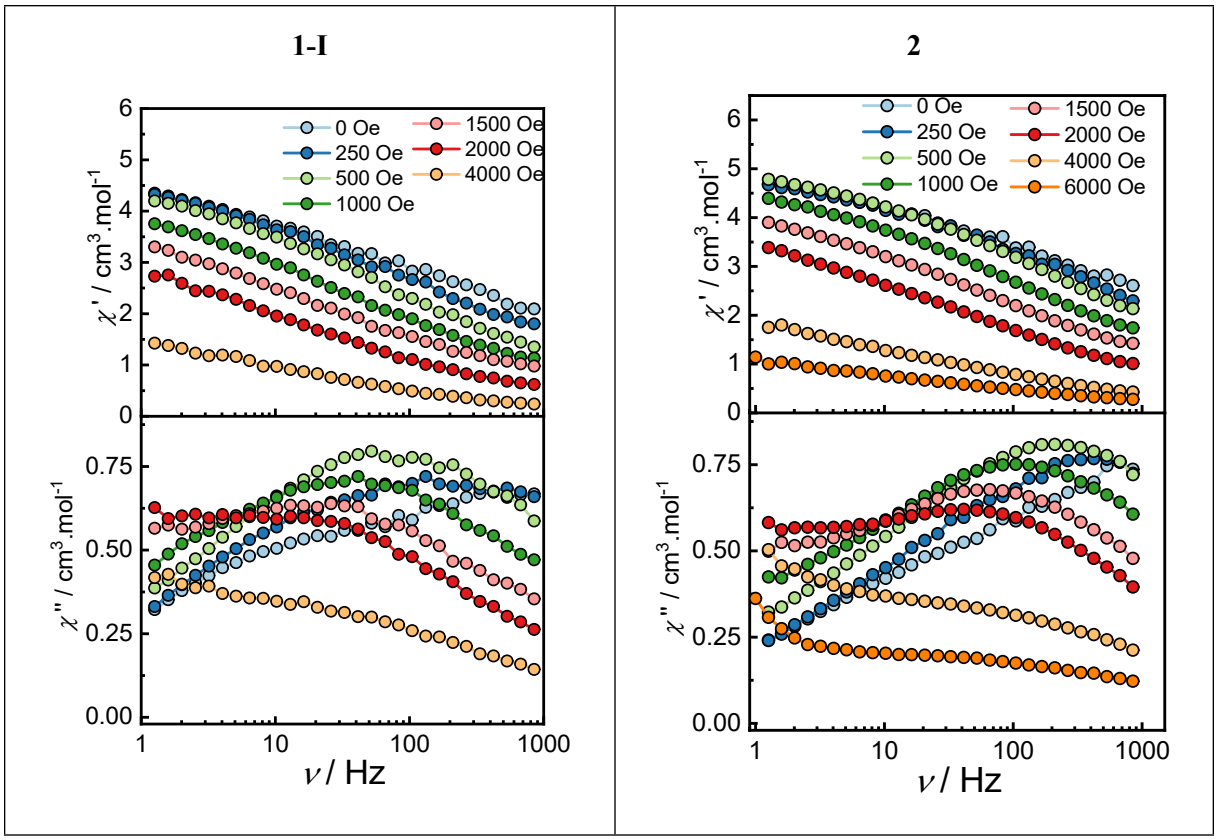

Figure S6: Frequency dependence of χ' and χ'' for **1** and **2** for various dc fields at 2 K.

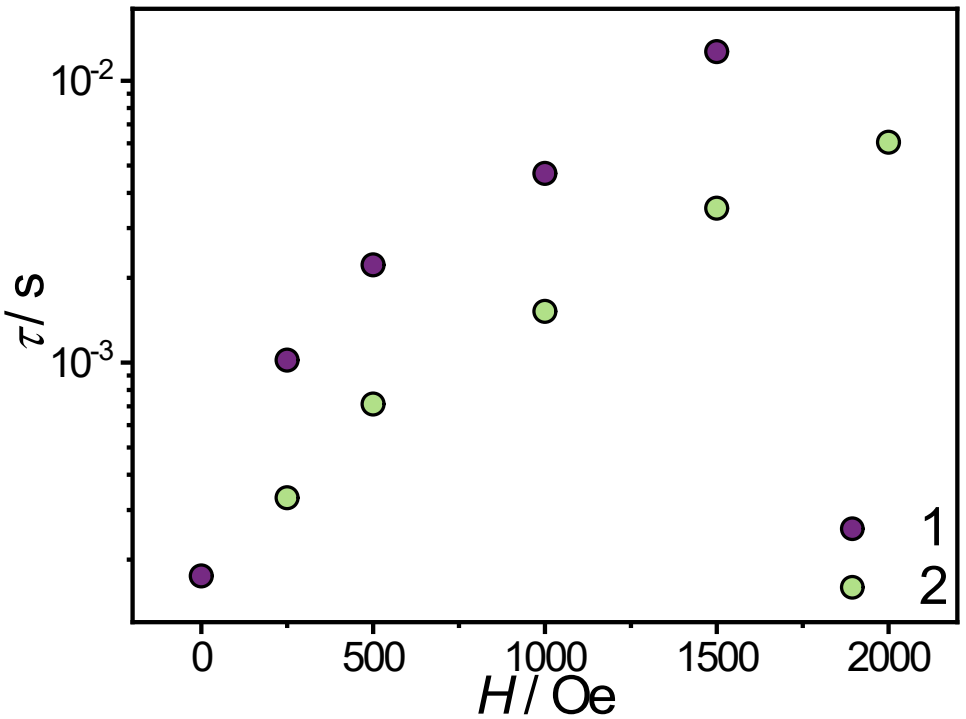

Figure S7: Field dependence of the relaxation time for **1** and **2** at 2 K.

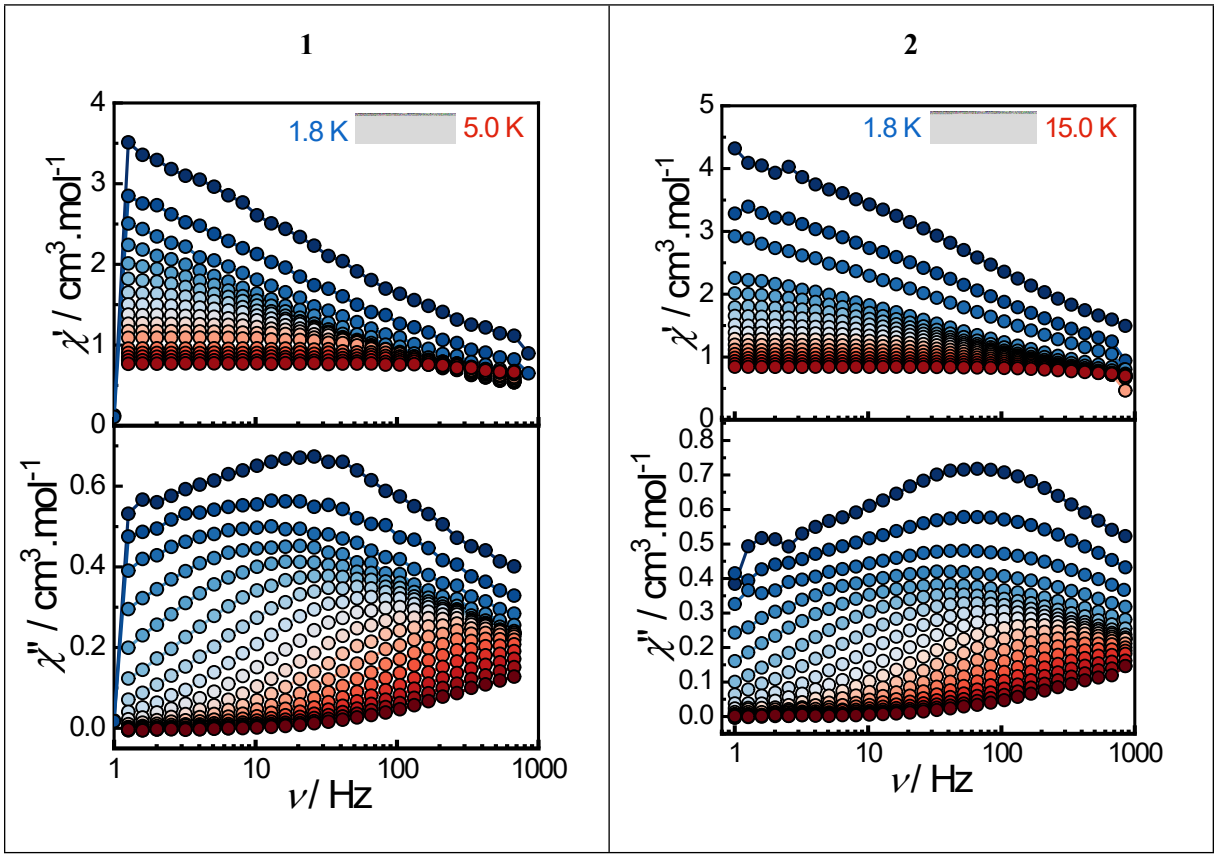

Figure S8: Frequency dependence of χ' and χ'' for **1**-I, **2**-Br under a 1500 Oe dc-field.

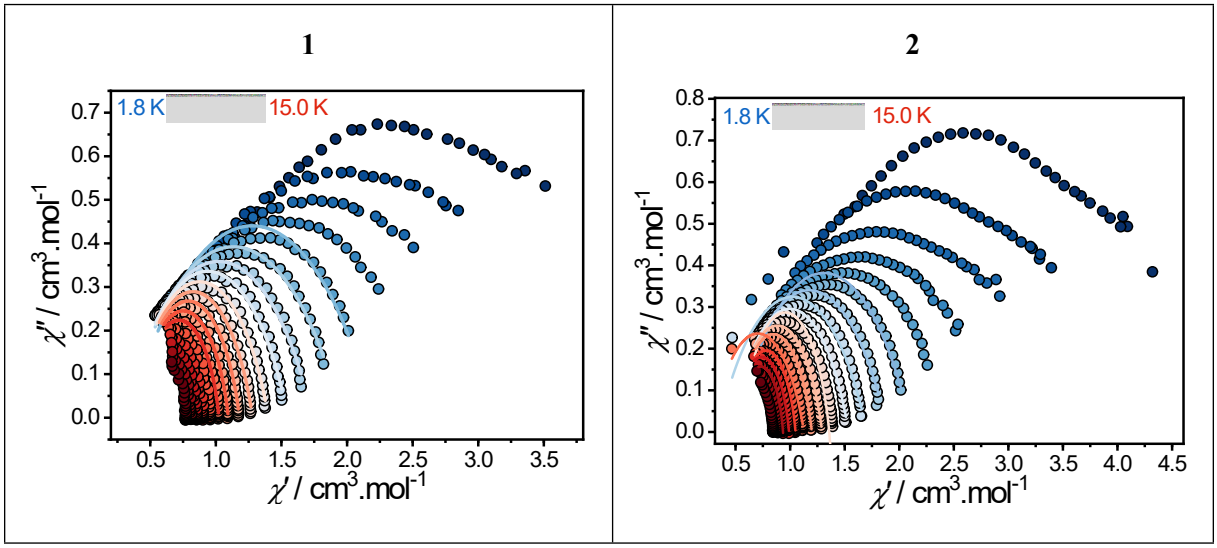

Figure S9: Cole-Cole (Argand) plots obtained using the ac susceptibility data for **1 and 2** under a 1500 Oe field. The solid lines represent the fit with a generalized Debye model.

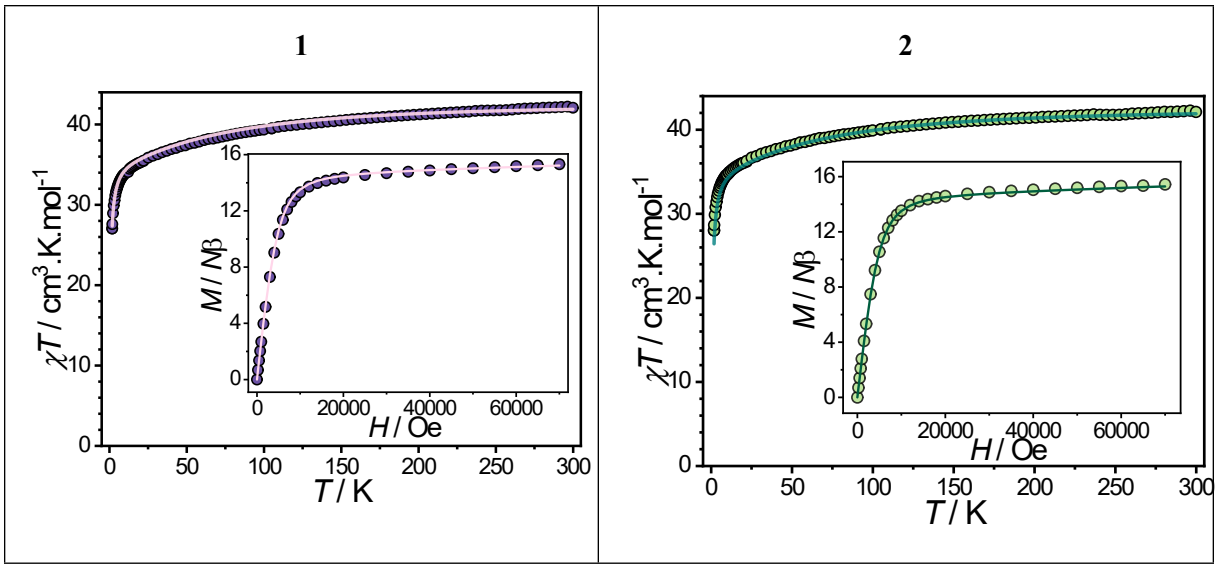

Figure S10: Temperature dependence of χT under an applied magnetic field of 1000 Oe for **1** and **2**. Inset: field dependence of the magnetization at 1.8 K. The solid lines represent the fit with POLY_ANISO.

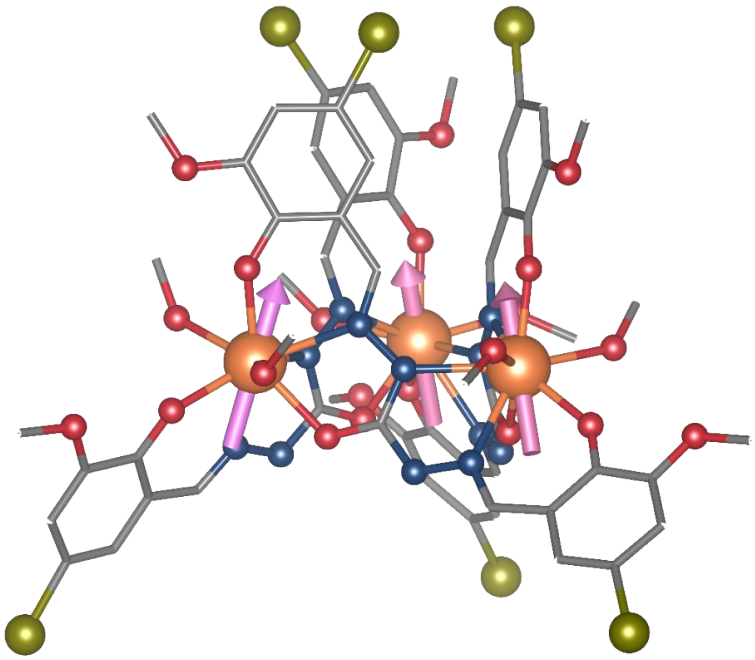

Figure S11: Orientation of the anisotropic axis (pink) corresponding to the ground KD in **2**.

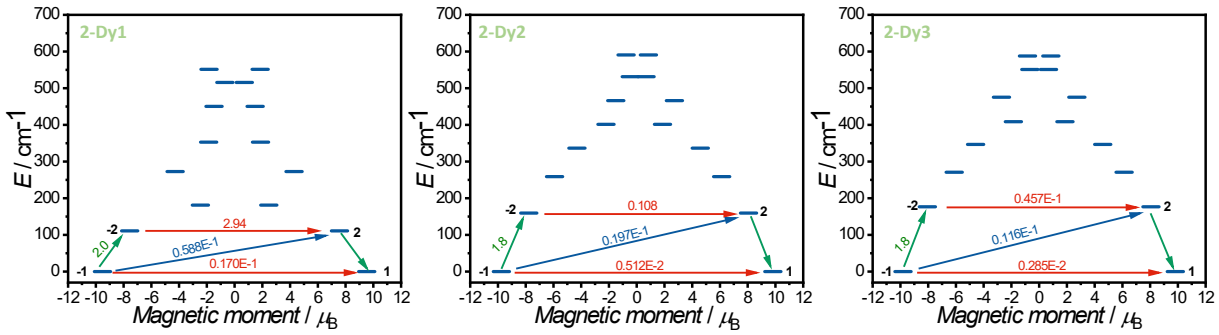

Figure S12: Energy diagram for low-lying KDs and transition magnetic moment matrix elements[1] (in μB) for the connected states (only for the KD1 and KD2) for fragments 1. For each KD (*n*), the corresponding states (–*n*, *n*) are placed according to their magnetic moments. The horizontal arrows show the QTM transitions within each doublet, whereas the non-horizontal arrows are spin-phonon transition paths. Only the first KDs are shown here.

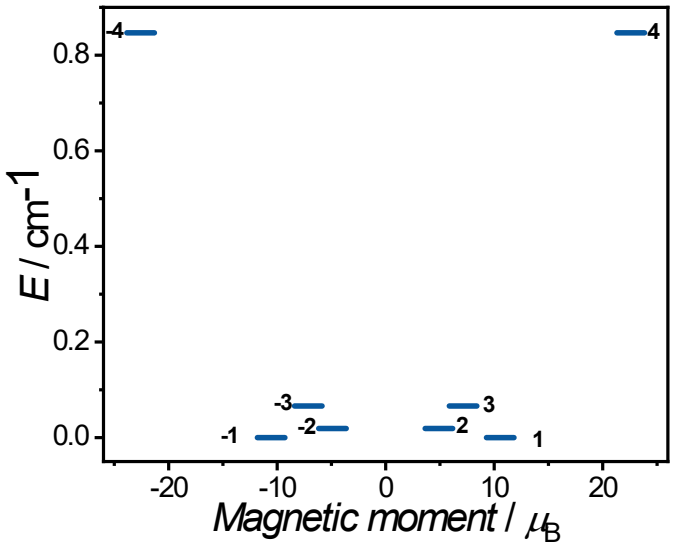

Figure S13: Energy diagram of the coupled states resulting from the dipolar interactions in **2**.

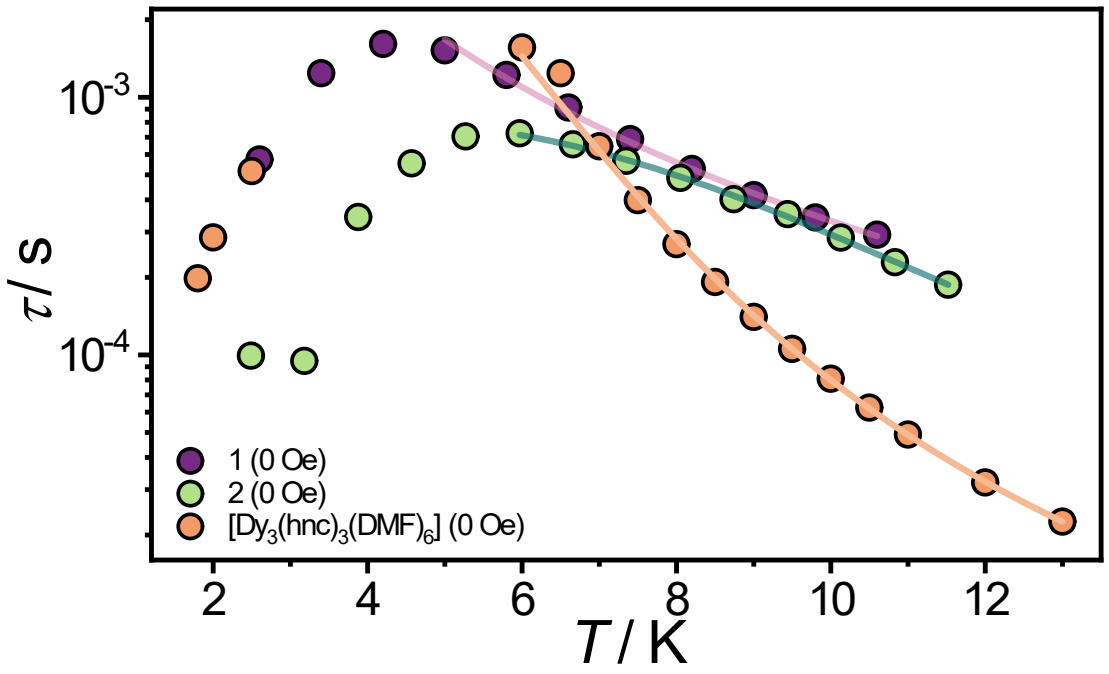

Figure S14: Temperature dependence of the relaxation time for $[Dy_3(hnc)_3(DMF)_6]$ using the ac susceptibility data.[2]

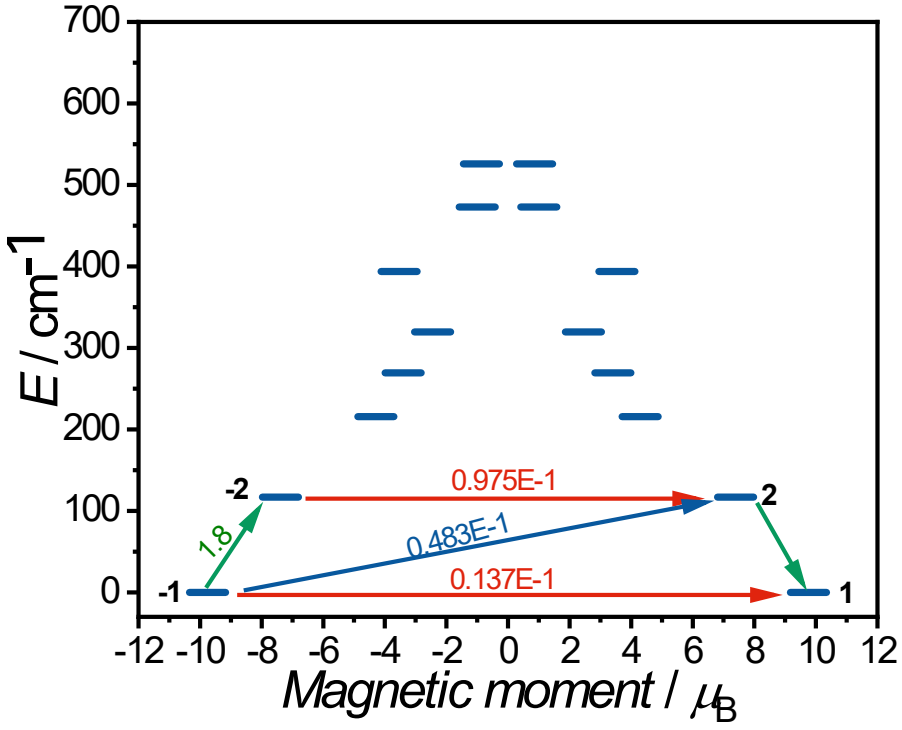

Figure S15: Energy diagram for low-lying KDs and transition magnetic moment matrix elements[1] (in μB) for the connected states (only for the KD1 and KD2) for fragments **$[Dy_3(hnc)_3(DMF)_6]$**. For each KD (n), the corresponding states ($-n$, n) are placed according to their magnetic moments. The horizontal arrows show the QTM transitions within each doublet, whereas the non-horizontal arrows are spin-phonon transition paths. Only the first KDs are shown here.

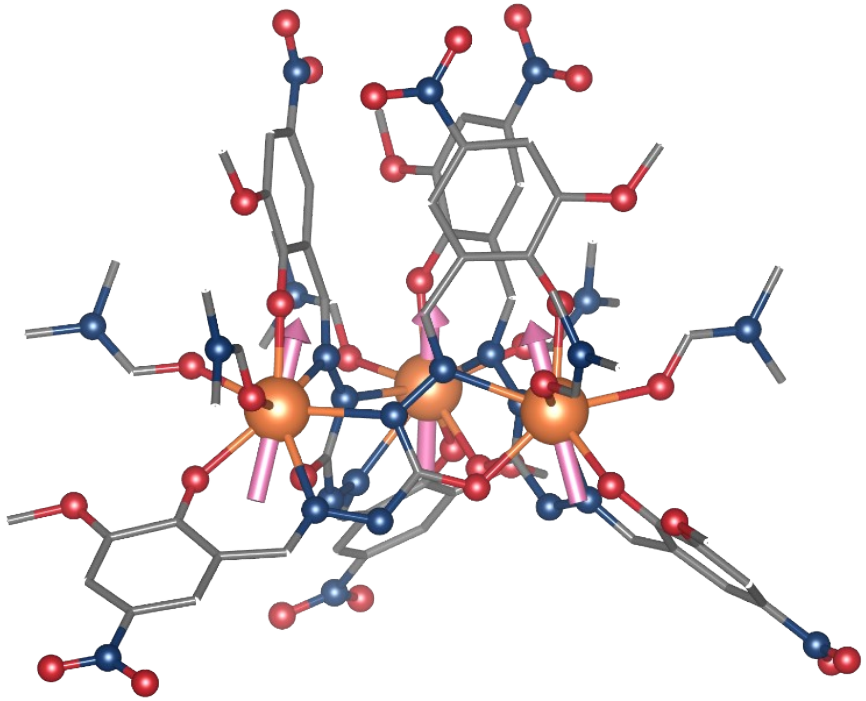

Figure S16: Orientation of the anisotropic axis (pink) corresponding to the ground KD in **[$Dy_3(hnc)_3(DMF)_6$]**.

Table S1: Crystal data, data collection and structure refinement details for **1-2**.

	1	**2**
Formula	$C_{64}H_{81}Dy_3N_{14}O_{26}I_6$	$C_{58}H_{70}Dy_3N_{12}O_{26}Br_6$
M	2713.73	2318.22
T, K	150.15 K	150.15 K
Crystal system	Triclinic	Triclinic
Space group	$P\bar{1}$	$P\bar{1}$
Z (*Z*')	2	2
a, Å	17.7191(19)	16.8007(12)
b, Å	17.8767(18)	16.9407(12)
c, Å	19.0135(18)	17.6129(11)
α, °	96.624(4)°	67.114(2)°
β, °	109.162(3)°	69.537(2)°
γ, °	116.283(4)°	77.110(2)°.
V, Å^3	4853.2(9)	4304.8(5)
d_{calcd}, g.cm^{-3}	1.857	1.788
Mu, mm^{-1}	4.271	5.435
F_{000}	2576	2236
wR_2 (all data)	0.2481	0.1116
$S(F^2)$	1.054	1.112

Table S2: SHAPE analysis for **1** and **2**.

		OP	HPY	HBPY	CU	SAPR	TDD	JGBF	JETBPY	JBTPR	BTPR	JSD	TT	ETBPY
1	Dy1	31.774	23.786	14.463	9.531	3.313	**1.222**	14.348	25.881	1.932	1.459	2.671	9.784	21.298
	Dy2	31.971	24.223	13.623	7.486	3.387	**0.793**	15.027	26.395	2.842	2.315	2.934	7.906	21.213
	Dy3	31.380	23.535	14.105	9.038	3.660	**1.345**	14.592	25.722	2.476	2.205	2.882	9.234	21.421
2	Dy1	30.144	24.447	13.633	7.201	2.703	**0.860**	14.810	26.395	3.162	2.869	2.972	7.545	21.206
	Dy2	32.296	23.324	15.057	9.010	2.919	**0.961**	14.709	26.831	2.025	1.431	2.783	9.432	21.981
	Dy3	32.711	23.142	15.216	10.385	3.319	2.075	14.146	25.547	2.098	**1.701**	4.450	10.566	21.343

OP: Octagon
HPY: Heptagonal pyramid
HBPY: Hexagonal bipyramid
CU: Cube
SAPR: Square antiprism
TDD: Triangular dodecahedron
JGBF: Johnson gyrobifastigium
JETBPY: Johnson elongated triangular bipyramid
JBTPR: Johnson biaugmented trigonal prism
BTPR: Biaugmented trigonal prism
JSD: Snub diphenoid J84
TT: Triakis tetrahedron
ETBPY: Elongated trigonal bipyramid

Table S3: Fitting of the Cole-Cole plots with a generalized Debye model under a 0 Oe dc field for 1.

T (K)	χ_S (cm^3. mol^{-1})	χ_T (cm^3. mol^{-1})	α
5.0	1.26741	1.49178	0.89182
5.8	1.15418	1.23867	0.95525
6.6	0.82495	1.33281	0.66394
7.4	0.69774	1.29431	0.50034
8.2	0.63878	1.22319	0.40425
9.0	0.5963	1.14213	0.34732
9.8	0.58161	1.08142	0.27898

Table S4: Fitting of the Cole-Cole plots with a generalized Debye model under a 0 Oe dc field for 1.

T (K)	χ_S (cm^3. mol^{-1})		χ_T (cm^3. mol^{-1})	α
6.66	1.09963		1.35278	0.83968
7.35	0.89966		1.38725	0.6166
8.05	0.81594		1.35691	0.46261
8.74	0.75752		1.28484	0.38911
9.44	0.6564		1.17331	0.42258
10.13	0.69063		1.15146	0.29463
10.83	0.65774		1.09017	0.26106
11.52	0.69279		1.06451	0.09199

Table S5: Fitting of the Cole-Cole plots with a generalized Debye model under a 1500 Oe dc field for 1.

T (K)	χ_S (cm^3. mol^{-1})	χ_T (cm^3. mol^{-1})	α
1.8	2.1114	2.59647	0.8788
2.576	1.6931	2.12925	0.87243
3.35	1.55184	1.74112	0.93791
4.13	1.27711	1.61391	0.87379
4.905	1.14749	1.4088	0.8903
5.682	1.01382	1.25476	0.88633
6.459	0.78423	1.25807	0.73541
7.235	0.62584	1.25415	0.56417
8.01	0.5546	1.19693	0.46196
8.788	0.51562	1.13499	0.38248
9.564	0.49811	1.08068	0.30408
10.341	0.48532	1.0192	0.26319
11.117	0.47606	0.96246	0.2376

Table S6: Fitting of the Cole-Cole plots with a generalized Debye model under a 1500 Oe dc field for 2.

T (K)	χ_S (cm^3. mol^{-1})	χ_T (cm^3. mol^{-1})	α
5.68234	1.22983	1.38729	0.92443
6.45915	1.13248	1.21767	0.95438
7.2333	0.94627	1.09613	0.91517
8.01197	0.72254	1.27294	0.56849
8.78767	0.64168	1.2664	0.26989
9.56401	0.61319	1.15525	0.40534
10.34038	0.59186	1.10074	0.33444
11.11687	0.47802	0.93034	0.54511
11.89339	0.56492	0.99077	0.25577
12.66963	0.54388	0.93561	0.25554
13.44628	0.56	0.89955	0.20017

Table S7: *Ab initio* calculated energies, *g*-tensor main values of the ground doublet and the nth KD doublet for the ground multiplet J = 15/2 obtained for the individual fragment **Dy1** in **1**.

KD	Energy (cm^{-1})	g_x	g_y	g_z	Wavefunction (only components with > 20 % are given)
1	0	0.01166107	0.02228686	19.3067124	88.8% |±15/2>
2	155.032	0.36233854	0.66874615	15.8018145	71.2% |±13/2>; 20.2% |±9/2>
3	247.057	1.57157479	2.55087407	14.5607962	30.3 % |±11/2>;24.4% |±7/2>
4	332.653	7.97476492	6.85010743	4.49152338	25.8 % |±7/2>
5	412.731	0.33042292	3.26661374	11.3609456	30.4 %|±9/2>
6	497.433	0.07221814	2.33375833	13.3184846	32.0% |±7/2>

7	543.867	1.04546893	1.52733438	16.1839127	35.8% | ±5/2>; 27.3% | ±3/2>
8	589.42	0.17497697	0.35982513	19.1758717	42.0 | ±1/2>; 30.2 | ±3/2>

Table S8: *Ab initio* calculated energies, *g*-tensor main values of the ground doublet and the nth KD doublet for the ground multiplet $J = 15/2$ obtained for the individual fragment **Dy2** in **1**.

KD	Energy (cm^{-1})	g_x	g_y	g_z	Wavefunction (only components with > 20 % are given)
1	0	0.00831479	0.01335843	19.5708357	93.7% | ±15/2>>
2	179.155	0.31858192	0.67977173	15.8432181	60.0% | ±13/2>; 27.0% | ±9/2>
3	253.192	0.71538859	1.60823598	14.3943246	41.1 % | ±11/2>; 33.6% | ±7/2>
4	343.399	3.69960238	5.2254283	9.91218785	30.0 % | ±5/2>; 23.7% | ±13/2>
5	417.773	1.7934997	5.41891051	10.8269826	22.5 % | ±11/2>; 21.1% | ±7/2>
6	485.76	0.77075762	3.30581252	14.8958021	29.3 % | ±5/2>; 22.6% | ±7/2>; 21.5% | ±9/2>
7	528.084	0.5906453	1.20658828	17.6439938	33.6% | ±3/2>; 23.8% | ±5/2>
8	606.154	0.07172542	0.22728275	18.5461544	61.5 | ±1/2>; 30.5 | ±3/2>

Table S9: *Ab initio* calculated energies, *g*-tensor main values of the ground doublet and the nth KD doublet for the ground multiplet $J = 15/2$ obtained for the individual fragment **Dy3** in **1**.

KD	Energy (cm^{-1})	g_x	g_y	g_z	Wavefunction (only components with > 20 % are given)
1	0	0.00836603	0.01698769	19.3313096	89.2% | ±15/2>>
2	139.800	0.32956999	0.65797745	15.3502712	64.5% | ±13/2>; 26.1% | ±9/2>
3	203.789	0.77760608	1.93215577	14.5719061	31.0 % | ±7/2>; 29.2% | ±11/2>
4	298.902	5.06532639	6.11739998	9.18741019	25.9 % | ±11/2>
5	377.058	0.08432191	4.12310942	11.1017355	33.2 % | ±9/2>
6	460.717	1.44506425	3.81855413	10.9838241	37.0 % | ±7/2>
7	501.929	2.02107085	3.79241359	13.5664982	34.9% | ±5/2>; 29.9% | ±3/2>
8	561.66	0.30377119	0.49981197	19.0740184	37.8% | ±1/2>; 30.2 | ±3/2>

Table S10: Anisotropic axis tilt in **1** and **2**.

Compound	Dy site	Dy-Dy vector	Angle (°)	Dy-Dy distance (Å)
1	Dy1	Dy1-Dy2	71.69	5.873
		Dy1-Dy3	78.01	5.772
	Dy2	Dy2-Dy1	77.93	5.873
		Dy2-Dy3	61.73	5.779
	Dy3	Dy3-Dy1	69.72	5.772
		Dy3-Dy2	78.92	5.779
2	Dy1	Dy1-Dy2	73.86	5.896
		Dy1-Dy3	85.94	5.798
	Dy2	Dy2-Dy1	67.46	5.758
		Dy2-Dy3	78.23	5.896
	Dy3	Dy3-Dy1	70.80	5.798
		Dy3-Dy2	78.30	5.758

Table S11: Dipolar interactions between the Dy^{3+} ions obtained from POLY_ANISO in **1.**

Compound			
Dy1-Dy2	1.03E-03	-1.54E-04	-4.81E-03
	-1.48E-03	2.23E-04	6.92E-03
	-1.67E-01	2.51E-02	7.81E-01
Dy1-Dy3	-1.23E-04	2.86E-04	-5.34E-03
	1.79E-04	-4.16E-04	7.81E-03
	2.00E-02	-4.64E-02	8.72E-01

Dy2-Dy3	4.11E-03	-9.43E-03	1.77E-01
	-6.19E-04	1.42E-03	-2.66E-02
	-1.92E-02	4.40E-02	-8.25E-01

Table S12: Exchange spectrum and g_z values obtained from POLY_ANISO for **1** and **2**.

Coupled state	Energy (cm^{-1}) **1**	g_z **1**	Energy (cm^{-1}) **2**	g_z **2**
1	0	23.7950	0	21.0972
2	0.023	21.5266	0.019	24.3439
3	0.037	24.4591	0.066	21.8148
4	0.859	53.7581	0.847	54.7755

Table S13: *Ab initio* calculated energies, *g*-tensor main values of the ground doublet and the nth KD doublet for the ground multiplet $J = 15/2$ obtained for the individual fragment **Dy1** in **2**.

KD	Energy (cm^{-1})	g_x	g_y	g_z	Wavefunction (only components with > 20 % are given)
1	0	0.0321791	0.07017251	19.0500416	84.4% |±15/2>>
2	110.997	0.61733327	1.10931365	15.6883623	66.0% |±13/2>;20.5% |±9/2>
3	181.09	0.78052535	2.56424002	16.4897122	23.5 % |±5/2>;21.3% |±7/2>
4	272.676	4.82145536	5.7450071	9.30101411	32.1 % |±11/2>
5	352.838	0.772571	3.36529846	11.8346291	33.3 % |±9/2>
6	450.338	0.9181531	1.44422074	13.6402774	33.3% |±7/2>; 21.4% |±1/2>
7	515.755	0.1494833	0.71751527	15.5930683	30.5% |±5/2>; 27.5% |±3/2>
8	551.449	0.10076942	0.38824654	18.332454	29.8% |±1/2>; 24.5% |±3/2>

Table S14: *Ab initio* calculated energies, *g*-tensor main values of the ground doublet and the nth KD doublet for the ground multiplet $J = 15/2$ obtained for the individual fragment **Dy2** in **2**.

KD	Energy (cm^{-1})	g_x	g_y	g_z	Wavefunction (only components with > 20 % are given)
1	0	0.01081664	0.01993828	19.5086855	92.6% |±15/2>>
2	159.423	0.23130059	0.39818364	16.3302879	70.5% |±13/2>

3	258.773	1.44535407	1.74580462	14.2475296	48.1% |±11/2>; 23.6% |±7/2>
4	336.499	4.27166572	5.8069663	9.07118574	24.3% |±9/2>; 20.2% |±5/2>
5	401.401	1.50484701	4.3667021	11.4198725	26.3% |±9/2>; 19.5% |±7/2>;19.3% |±11/2>
6	466.139	0.63168363	2.16209173	15.3623193	34.4% |±7/2>; 26.5% |±5/2>
7	531.387	0.25491982	0.92299019	17.5556212	33.6% |±3/2>; 31.5% |±5/2>
8	590.597	0.1698793	0.44178764	18.433045	58.5% |±1/2>; 32.6% |±3/2>

Table S15: *Ab initio* calculated energies, *g*-tensor main values of the ground doublet and the nth KD doublet for the ground multiplet $J = 15/2$ obtained for the individual fragment **Dy3** in **2**.

KD	Energy (cm^{-1})	g_x	g_y	g_z	Wavefunction (only components with > 20 % are given)
1	0.0	0.00770221	0.0094397	19.6217717	94.4% |±15/2>
2	176.661	0.08418776	0.17530077	16.5870212	80.9% |±13/2>
3	270.921	0.42831418	0.55260511	15.37954984	50.7% |±11/2>
4	346.656	4.43369329	5.81866247	9.18471947	23.0% |±7/2>; 21.8% |±9/2>
5	408.755	2.16928708	4.40980029	11.63110424	23.8 % |±9/2>
6	475.464	0.01615021	1.20620884	16.19936106	39.0% |±7/2>
7	551.022	1.26646987	1.8921333	14.59983488	34.4% |±5/2>; 26.7% |±3/2>;24.8% |±1/2>
8	587.805	0.62207382	3.09841846	16.2252042	50.3% |±1/2>; 36.0% |±3/2>

Table S16: Dipolar interactions between the Dy^{3+} ions obtained from POLY_ANISO in **2.**

Compound			
Dy1-Dy2	3.02E-06	5.50E-05	-3.33E-04
	-1.78E-04	-3.11E-03	1.85E-02
	-7.39E-03	-1.26E-01	7.50E-01
Dy1-Dy3	6.84E-07	1.42E-06	-5.02E-05

	-6.46E-04	-3.90E-04	1.97E-02
	-2.61E-02	-1.58E-02	7.99E-01
Dy2-Dy3	-2.86E-04	-1.74E-04	8.73E-03
	-4.85E-03	-2.95E-03	1.48E-01
	2.89E-02	1.75E-02	-8.80E-01

Table S17: *Ab initio* calculated energies, *g*-tensor main values of the ground doublet and the nth KD doublet for the ground multiplet $J = 15/2$ obtained for **[Dy$_3$(hnc)$_3$(DMF)$_6$].**

KD	Energy (cm^{-1})	g_x	g_y	g_z	Wavefunction (only components with > 20 % are given)
1	0	0.02608356	0.05640261	19.513229	93.3% |±15/2>
2	116.834	0.24917351	0.2986095	16.6866564	66.8% |±13/2>
3	215.606	1.82591064	3.1773713	12.2881168	25.5 % |±13/2>
4	269.336	0.89154121	4.80950394	8.92257423	43.4% |±11/2>
5	319.658	4.05557589	4.22227126	11.87412	29.5 % |±9/2>;23.2% |±5/2>
6	393.835	0.50241169	0.86319255	17.2662136	36.0% |±7/2>; 30.3% |±9/2>
7	472.948	0.12230369	0.32737801	18.9083867	29.6% |±3/2>; 28.3% |±5/2>
8	525.853	0.02620209	0.19568948	19.3696922	41.7 % |±1/2>;28.5% |±3/2>

References

1. L. Ungur and L. F. Chibotaru, *Inorg. Chem.*, 2016, **55**, 10043-10056.
2. L.-W. Cheng, C.-L. Zhang, J.-Y. Wei and P.-H. Lin, *Dalton Trans.*, 2019, **48**, 17331-17339.